Electrical tuning of emissivity and linewidth of thermal emission spectra

Takuya Inoue,* Menaka De Zoysa, Takashi Asano, and Susumu Noda
Department of Electronic Science and Engineering, Kyoto University, Kyoto-Daigaku-Katsura, Nishikyo-ku, Kyoto 615-8510, Japan
(Received 25 February 2015; revised manuscript received 11 May 2015; published 18 June 2015)

Here, we report on the postfabrication tuning of thermal emission spectra using photonic crystal resonators interacting with n-type quantum wells. Our method is based on the voltage control of intersubband absorption in the quantum wells, which allows the continuous tuning of both the thermal emission intensity and the linewidth. By adjusting an applied bias to match the intersubband absorption rate with the radiative rate of the resonator, we realize the maximization of the emissivity (0.7) of a narrowband thermal emission peak ($Q = 157$). Even narrower thermal emission ($Q > 200$) is also demonstrated with the same device by increasing the applied bias.

DOI: 10.1103/PhysRevB.91.235316 PACS number(s): 42.70.Qs, 44.40.+a, 78.67.De

I. INTRODUCTION

Thermal emitters generally exhibit a broad spectrum, ranging from the terahertz to the visible, and are used for various applications, including chemical analysis [1], gas sensing [2], and thermophotovoltaics [3–5]. As these applications require a limited spectral bandwidth (e.g., corresponding to a Q factor of ∼50–100 in the case of nondispersive infrared sensing) [2], it is highly desirable to realize narrowband thermal emission concentrated within a target bandwidth for each application to improve the efficiency of power utilization. Recently, thermal emission control with optical resonators has been intensively investigated [6–13], and spectra with various linewidth and emissivity values have been realized, depending on the absorptive and radiative properties of the resonators [14]. For example, metallic resonators [6–10] exhibited broad emission peaks ($Q < 10$) due to their strong absorption in metal, whereas dielectric emitters [11–13] realized narrower emission peaks ($Q \sim 100$) with suppressed background emission. However, in those emitters demonstrated so far, the absorptive properties have been fixed by the materials used, and the radiative properties have been also fixed by the structures used. The postfabrication tuning of the spectral features of controlled thermal emission has, thus, not yet been reported.

On the other hand, we recently demonstrated the dynamic control of thermal emission by using intersubband transitions (ISB-Ts) in multiple quantum wells (MQWs) and an in-plane optical resonance of a photonic crystal (PC) slab [15]. The emitter allowed the electrical control of the ISB absorption in the MQWs, thereby realizing the ultrafast switching of thermal emission intensity. Here, we use this electrical controllability to demonstrate the postfabrication tuning of emissivity and linewidth for ultra-narrowband high-emissivity thermal emission. The maximization of the peak emissivity in each device is realized by matching the ISB absorption rate with the radiation rate of the PC resonance, and a narrowband thermal emission peak with a variable linewidth ($Q = \sim 120-200$) is demonstrated.

II. THEORY AND DESIGN OF THERMAL EMITTERS

As mentioned, the key to realizing the precise control of the spectral features of thermal emission with an optical resonator lies in adjusting its absorptive and radiative properties. The emissivity spectrum obtained from a single resonator at an angular frequency of ω_{res} is theoretically derived as

$$\varepsilon(\omega) = \varepsilon_{max} \times \frac{1/Q_{abs}Q_{rad}}{(\omega/\omega_{res} - 1)^2 + (1/2Q_{abs} + 1/2Q_{rad})^2}, \quad (1)$$

where Q_{abs} and Q_{rad} are the Q factors of the resonator, which are determined by the decay rates of the modal electric field due to the material's absorption and far-field radiation, respectively [16–21]. ε_{max} is equal to 1 when the resonator couples to a single radiation channel, whereas it decreases when the mode couples to multiple radiation channels [20]. Equation (1) shows that the peak emissivity $\varepsilon(\omega_{res})$ takes the maximum value (ε_{max}) when Q_{abs} and Q_{rad} are equal (Q matching), whereas it decreases as they diverge due to the impedance mismatching of the power transfer between the absorber and the output channel of the resonator. The Q factor of the thermal emission spectrum is given by $(Q_{abs}^{-1} + Q_{rad}^{-1})^{-1}$, which becomes higher as Q_{abs} and Q_{rad} increase. Therefore, by externally changing the value of either Q_{abs} or Q_{rad}, we can realize a thermal emission spectrum with a high peak emissivity and a flexible linewidth.

Figure 1(a) shows the structure of a narrowband thermal emitter designed for this purpose. The emitter consists of 10-layer GaAs/$Al_{0.3}Ga_{0.7}As$ MQWs grown between a p-type GaAs layer and an n-type GaAs layer, in which a triangular lattice of air holes is introduced to form a PC slab structure [15]. Each QW layer consists of a 6.8 nm undoped GaAs well and a 13.0 nm n-doped $Al_{0.3}Ga_{0.7}As$ barrier. This device yields a narrowband emissivity (absorptivity) spectrum owing to the combination of ISB-Ts of the MQW layers [22], which has a limited spectral bandwidth and an in-plane optical resonance of the PC slab, achieving efficient coupling of ISB-Ts to far-field radiation [12,13]. The central wave number and full width at half maximum (FWHM) of the ISB-Ts are 1090 and 75 cm^{-1}, respectively. The far-field radiation rate of the in-plane resonant mode of the PC (which is inversely proportional to Q_{rad}) is determined by the air-hole size of the PC slab. Figure 1(b) shows the Q_{rad} of one of the PC resonant modes as a function of the air-hole radius (r), calculated by using the three-dimensional finite-difference

*t_inoue@qoe.kuee.kyoto-u.ac.jp

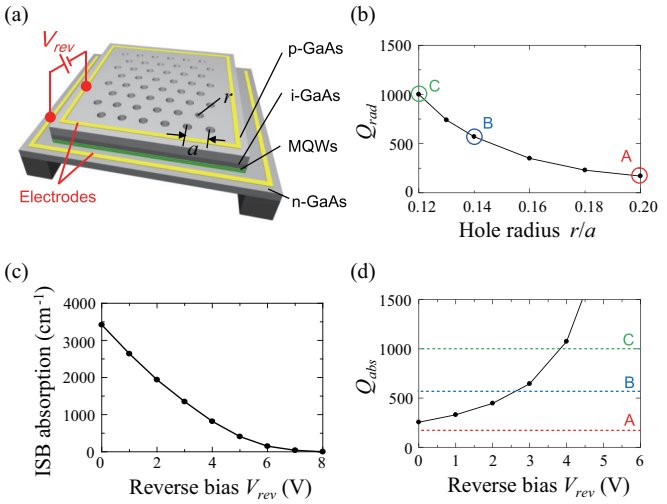

FIG. 1. (Color online) (a) Schematic of the electrically controllable thermal emitter, which consists of a p-i-n GaAs diode incorporating GaAs/$Al_{0.3}Ga_{0.7}As$ MQWs and a two-dimensional PC slab. The thicknesses of the p-type GaAs layer, the intrinsic GaAs layer, the MQW layer, and the n-type GaAs layer are 800, 200, 200, and 800 nm, respectively. The $Al_{0.3}Ga_{0.7}As$ barrier layer is doped with silicon at a density of 1.0×10^{17}cm^{-3}. (b) Calculated radiative Q factor ($Q_{\rm rad}$) of a resonant mode in the PC slab as a function of r. Circles show the r values of the fabricated emitters (A, B, and C). (c) Calculated ISB absorption coefficient of the MQWs as a function of reverse bias. (d) Calculated absorptive Q factor ($Q_{\rm abs}$) of the same resonant mode as a function of reverse bias. The dotted lines show the calculated radiative Q factor of the fabricated emitters.

time-domain (3D-FDTD) method, in which a smaller r leads to a higher $Q_{\rm rad}$ (i.e., a weaker coupling strength). The absorption loss rate of the in-plane resonant mode (which is inversely proportional to $Q_{\rm abs}$) is determined by the ISB absorption of the MQWs, which is tunable by a reverse bias applied to the p-n junction that changes the electron density in the first subband of the MQWs. Figure 1(c) shows the voltage-dependent ISB-absorption coefficient ($\alpha_{ISB\text{-}T}$) at the transition wavelength, calculated by solving the Schrödinger equation and Poisson's equation self-consistently. The value of the absorption coefficient changes from 3500 cm^{-1} to almost 0 cm^{-1}, as the reverse bias increases from 0 to 8 V. The relationship between $\alpha_{ISB\text{-}T}$ and $Q_{\rm abs}$ is given by

$$Q_{\rm abs} = \frac{\omega_{\rm res} n_{MQW}}{c \Gamma \alpha_{ISB\text{-}T}}, \qquad (2)$$

where n_{MQW} is a refractive index of the MQWs, c is the speed of light in vacuum, and Γ is the optical confinement factor of the resonant mode in the QW layer (~2.5%). The corresponding $Q_{\rm abs}$ as a function of reverse bias is shown in Fig. 1(d). The value of $Q_{\rm abs}$ at zero bias is 250, and it rapidly increases as the reverse bias increases, leading to a narrower linewidth of the controlled thermal emission spectrum, according to Eq. (1). Note, however, that free carriers in the doped contact layers also cause small but nonzero optical absorption, which limits the maximum value of $Q_{\rm abs}$ to several thousand.

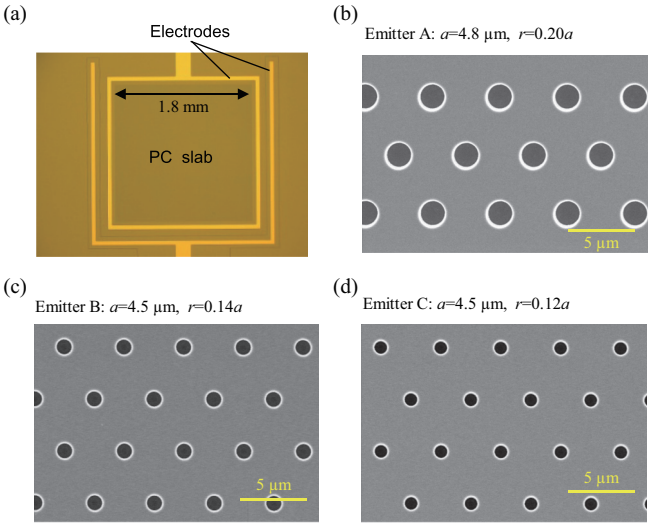

FIG. 2. (Color online) (a) Optical microscope image of the fabricated thermal emitter with a PC slab and p-type/n-type Ohmic electrodes. (b)–(d) Scanning electron microscope image of the air-hole patterns of the emitters A, B, and C.

III. EXPERIMENTAL RESULTS

Taking account of the calculated $Q_{\rm abs}$ and $Q_{\rm rad}$ values shown in Fig. 1, we fabricated three thermal emitters (A, B, and C) with different r values and lattice constants (a). The fabrication process was as detailed by the previous paper [15]. An optical microscope image of the fabricated device is shown in Fig. 2(a), and scanning electron microscope images of the PC patterns of the three emitters are shown in Figs. 2(b)–2(d). The r values of the emitters A, B, and C were set to 0.20a, 0.14a, and 0.12a, respectively, and the a values of the PC patterns were adjusted so that the frequency of the PC resonant modes coincided with the ISB-T frequency. The calculated value of $Q_{\rm rad}$ for each emitter shown in Fig. 1(b) was included for comparison in Fig. 1(d) (dotted lines). As mentioned, the peak emissivity of each emitter is expected to reach a maximum value at the point where the solid curve ($Q_{\rm abs}$) crosses each dotted line ($Q_{\rm rad}$).

For characterization of the fabricated thermal emitters, each was placed on top of an external heater at 200 °C, and the thermal emission spectra were measured with a Fourier-transform infrared spectrometer, changing the applied reverse bias from 0 to 10 V. The measured emission spectra corresponded to the integrated emission of all polarizations within a radiation angle of 3° to the surface normal direction. Figures 3(a), 3(c), and 3(e) show the entire thermal emission spectra of the three emitters with and without a reverse bias of 10 V (note that the reverse bias of 10 V completely depleted the MQWs). The thermal emission spectra of the reference blackbody at the same temperature are also plotted for comparison. All three emitters showed a sharp peak around the wave number of the ISB-T (1090 cm^{-1}). The peak intensity decreased with a reverse bias of 10 V but did not vanish due to the free-carrier absorption (emission) in the doped layers. Note that there were several smaller side peaks in addition to the main peak, which were caused by the other resonant modes of the PC slab. However, their intensity change caused by the

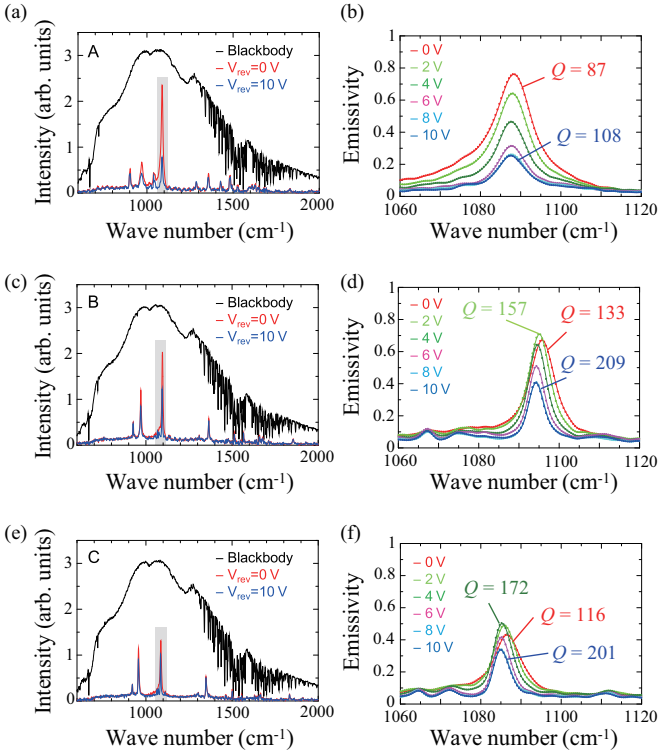

FIG. 3. (Color online) (a), (c), and (e) Measured thermal emission spectra of the fabricated thermal emitters (A, B, and C) at 200 °C with and without a reverse bias of 10 V. The thermal emission spectrum of a blackbody reference sample of the same area at the same temperature is also shown. (b), (d), and (f) Magnified emissivity spectra of the narrowband thermal emission peaks, corresponding to the shaded area in (a), (c) and (e) at different values of reverse bias.

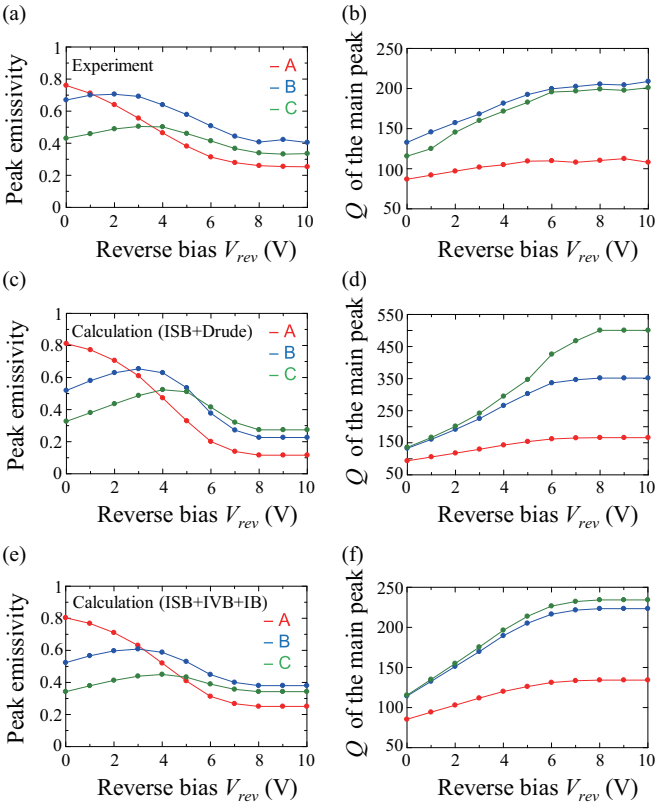

FIG. 4. (Color online) Peak emissivities and Q factors of the main thermal emission peaks of the fabricated emitters as a function of reverse bias. (a) and (b) Experimental results. (c) and (d) Calculations taking account of ISB absorption and Drude-like free-carrier absorption. (e) and (f) Calculations taking account of ISB absorption, IVB absorption, and IB caused by spatial nonuniformity in the r values.

reverse bias was smaller than that of the main peak due to the larger frequency detuning from the ISB-T. For example, in the case of the side emission peak at the wave number of 970 cm^{-1}, the ISB absorption coefficient there at zero bias (~300 cm^{-1}) is equal to the one at the main peak at a reverse bias of 5.5 V [see Fig. 1(c)]. Therefore, the amount of the intensity change of the side peak under the bias increasing from 0 to 10 V was comparable to that of the main peak under the bias increasing from 5.5 to 10 V.

Figures 3(b), 3(d), and 3(f) show the detailed spectral evolution of the main thermal emission peak of each emitter with various reverse biases. In the case of emitter A, the thermal emission intensity monotonically decreased as the reverse bias was increased to 8 V, at which point the electrons were completely extracted from the MQWs. By contrast, emitter B showed a higher thermal emission intensity at a reverse bias of 2 V than that without reverse bias. This result indicates the satisfaction of the Q-matching condition at 2 V, which is consistent with the calculated result shown in Fig. 1(d). Similarly, the peak emissivity of emitter C increased initially as the reverse bias was increased to 4 V, and then decreased with larger bias, which also agrees well with the result shown in Fig. 1(d). Closer examination of the thermal emission spectra in the Q-matching condition revealed that emitter B simultaneously realized a high Q factor (157) and a high emissivity (0.7), whereas emitter C realized an even high Q factor (172) with an emissivity of 0.5. These values significantly exceed those of the narrowband thermal emitters we previously reported ($Q = 107$, $\varepsilon = 0.4$) [13] in which the matching between Q_{abs} and Q_{rad} was not perfect due to the lack of a tuning method after fabrication.

IV. DISCUSSION

Here, we make a detailed comparison between the experimental results and the calculated results. Figures 4(a) and 4(b) show the peak emissivities and Q factors of the main thermal emission peaks, shown in Fig. 3, as a function of reverse bias. Figures 4(c) and 4(d) show the corresponding results calculated by rigorous coupled wave analysis (RCWA), which takes account of the ISB-absorption coefficients, shown in Fig. 1(c), and free-carrier absorption, described by the Drude model. Comparing both the experimental and calculated results in Figs. 4(a) and 4(c) indicates a monotonic decrease of emissivity in the case of emitter A and maximum values at nonzero bias in the case of emitters B and C. The reverse bias values at which the emissivity reached a maximum in the experimental results (0 V for A, 2 V for B, and ~3−4 V for C) were in good agreement with those from the calculations (0 V

for A, 3 V for B, and 4 V for C). The value of the maximum emissivity at the Q-matching decreases as the air-hole radius becomes smaller, the reason for which can be explained as follows. As we have mentioned in Sec. II, peak emissivity at the Q-matching condition ($\varepsilon_{\max}$) is determined by the number of radiation channels the mode couples to. In the case of our device, the mode can couple to both upward and downward radiation but selectively radiates upward owing to a PC pattern introduced in the upper part of the structure. When the air-hole radius is too small, however, the vertical asymmetry of the structure is lost, and thus the upward emissivity decreases.

As for the voltage dependence of the Q factor of the main peak [Fig. 4(b) and Fig. 4(d)], each emitter exhibited a monotonic increase of Q with greater reverse bias, thereby realizing the postfabrication tuning of the thermal emission linewidth. The maximum experimental Q factor (that was obtained at a reverse bias of 10 V for emitters B and C) was over 200, which was twice that of our previously reported emitter [13].

Note that there were some discrepancies between the experimental and calculated results, especially at reverse bias values larger than 6 V: specifically, the peak emissivity of the fabricated emitters was higher in the experimental results than in the calculated results, whereas the Q factors were lower. The higher peak emissivity at large reverse bias values (which turned off the ISB absorption) suggests that the optical absorption caused by the doped free carriers in the fabricated devices is larger than that assumed in the Drude model. For example, the intervalence-band (IVB) absorption by the holes in the p-type GaAs layer [23] can have an optical absorption coefficient of around $100\,\mathrm{cm}^{-1}$ in this spectral range, which has a large impact on the peak emissivity when the ISB absorption is turned off. Such residual absorption also leads to the broadening of the main peak; yet, even if the IVB absorption is included, the Q factors of emitters B and C at a reverse bias of 10 V are estimated to be higher than 350. Therefore, we infer that the lower experimental Q factors ($\sim$200) are mainly caused by the inhomogeneous broadening (IB) of the thermal emission peaks due to the spatial nonuniformity of r values in the millimeter scale PC slab ($1.8 \times 1.8\,\mathrm{mm}^2$). The RCWA calculation reveals that the assumption of the IVB-absorption coefficient of around $70\,\mathrm{cm}^{-1}$ and the standard deviation of 12 nm in the r values (which can arise during the fabrication process) reproduces the experimental results well, as shown in Figs. 4(e) and 4(f).

V. CONCLUSION

We have demonstrated the postfabrication tuning of the emissivity and linewidth of thermal emission spectra by using electrically controllable narrowband thermal emitters combining MQWs and PC slabs. By adjusting a reverse bias to satisfy the Q matching between absorption and radiation, we have realized a narrowband ($Q = 157$) high-emissivity ($\sim$0.7) thermal emission peak. Further narrowing of the thermal emission peak ($Q > 200$) has also been achieved by simply increasing the reverse bias. These flexible features will be suitable for a number of practical applications, including chemical analysis and gas sensing. From the viewpoint of fundamental science, the Q matching between absorption and radiation, which we have experimentally demonstrated here, is an underlying physical phenomenon not only for thermal emitters but also for other optical devices, such as wave absorbers [24] and solar cells [25]. We hope that our demonstration will also contribute to a deeper understanding of device physics and provide clear guidelines for the design of various optical devices.

ACKNOWLEDGMENTS

This paper was partially supported by a Grant-in-Aid for Scientific Research (25220607) from the Japan Society for the Promotion of Science (JSPS) and Core Research for Evolutional Science and Technology (CREST) from the Japan Science and Technology Agency (JST). T.I. also acknowledges support from a research fellowship of the JSPS.

[1] B. Stuart, *Infrared Spectroscopy: Fundamentals and Applications* (Wiley, Chichester, United Kingdom, 2004).
[2] J. Hodgkinson and R. P. Tatam, Meas. Sci. Technol. **24**, 012004 (2013).
[3] R. M. Swanson, Proc. IEEE **67**, 446 (1979).
[4] H. Sai and H. Yugami, Appl. Phys. Lett. **85**, 3399 (2004).
[5] A. Lenert, D. M. Bierman, Y. Nam, W. R. Chan, I. Celanovic, M. Soljačić, and E. N. Wang, Nat. Nanotechnol. **9**, 126 (2014).
[6] S. Y. Lin, J. Moreno, and J. G. Fleming, Appl. Phys. Lett. **83**, 380 (2003).
[7] V. Rinnerbauer, Y. X. Yeng, W. R. Chan, J. J. Senkevich, J. D. Joannopoulos, M. Soljačić, and I. Celanovic, Opt. Express **21**, 11482 (2013).
[8] K. Ikeda, H. T. Miyazaki, T. Kasaya, K. Yamamoto, Y. Inoue, K. Fujimura, T. Kanakugi, M. Okada, K. Hatade, and S. Kitagawa, Appl. Phys. Lett. **92**, 021117 (2008).
[9] I. Puscasu and W. L. Schaich, Appl. Phys. Lett. **92**, 233102 (2008).
[10] X. Liu, T. Tyler, T. Starr, A. F. Starr, N. M. Jokerst, and W. J. Padilla, Phys. Rev. Lett. **107**, 045901 (2011).
[11] J.-J. Greffet, R. Carminati, K. Joulain, J.-P. Mulet, S. Mainguy, and Y. Chen, Nature (London) **416**, 61 (2002).
[12] M. D. Zoysa, T. Asano, K. Mochizuki, A. Oskooi, T. Inoue, and S. Noda, Nat. Photonics **6**, 535 (2012).
[13] T. Inoue, M. D. Zoysa, T. Asano, and S. Noda, Appl. Phys. Lett. **102**, 191110 (2013).
[14] T. Inoue, M. D. Zoysa, T. Asano, and S. Noda, Optica **2**, 27 (2014).
[15] T. Inoue, M. D. Zoysa, T. Asano, and S. Noda, Nat. Mater. **13**, 928 (2014).
[16] I. Celanovic, D. Perreault, and J. Kassakian, Phys. Rev. B **72**, 075127 (2005).
[17] D. L. C. Chan, I. Celanovic, J. D. Joannopoulos, and M. Soljačić, Phys. Rev. A **74**, 064901 (2006).
[18] T. Asano, K. Mochizuki, M. Yamaguchi, M. Chaminda, and S. Noda, Opt. Express **17**, 19190 (2009).

[19] L. Zhu, S. Sandhu, C. Otey, S. Fan, M. B. Sindair, and T. S. Luk, Appl. Phys. Lett. **102**, 103104 (2013).
[20] T. Inoue, T. Asano, M. D. Zoysa, A. Oskooi, and S. Noda, J. Opt. Soc. Am. B **30**, 165 (2013).
[21] M. Ghebrebrhan, P. Bermel, Y. X. Yeng, I. Celanovic, M. Soljačić, and J. D. Joannopoulos, Phys. Rev. A **83**, 033810 (2011).
[22] L. C. West and S. J. Eglash, Appl. Phys. Lett. **46**, 1156 (1985).
[23] J. S. Blakemore, J. Appl. Phys. **53**, R123 (1982).
[24] R. Kakimi, M. Fujita, M. Nagai, M. Ashida, and T. Nagatsuma, Nat. Photonics **8**, 657 (2014).
[25] H. Shigeta, M. Fujita, Y. Tanaka, A. Oskooi, H. Ogawa, Y. Tsuda, and S. Noda, Appl. Phys. Lett. **101**, 161103 (2012).